Optical spectroscopy study of the topological property in PrSb

W. J. Ban,[1] D. S. Wu,[2,3] C. C. Le,[4,5] J. P. Hu,[5,4,6] J. L. Luo,[2,3] and H. Xiao[1,*]

[1]*Center for High Pressure Science and Technology Advanced Research, Beijing 100094, China*

[2]*Beijing National Laboratory for Condensed Matter Physics, Institute of Physics, Chinese Academy of Sciences, P.O. Box 603, Beijing 100190, China*

[3]*School of Physical Sciences, University of Chinese Academy of Sciences, Beijing 100049, China*

[4]*Kavli Institute for Theoretical Sciences and CAS Center for Excellence in Topological Quantum Computation, University of Chinese Academy of Sciences, Beijing 100190, China*

[5]*Beijing National Research Center for Condensed Matter Physics and Institute of Physics, Chinese Academy of Sciences, Beijing 100190, China*

[6]*South Bay Interdisciplinary Science Center, Dongguan, Guangdong Province 523808, China*

(Received 22 March 2019; published 16 September 2019)

We report an optical spectroscopy study of a single-crystal sample of PrSb, one of the monoantimonide *R*Sb compounds, which show interesting properties, such as topological nontrivial surface states and extremely large magnetoresistance. The plasma frequency is revealed at about 4300 cm^{-1}, suggesting a low carrier density. In addition, we found two quasilinear components with variable slopes in the real part of the optical conductivity $\sigma_1(\omega)$. In combination with theoretical calculations which reveal a band inversion, our results may provide optical spectroscopic evidence of a topological nontrivial property in PrSb.

DOI: 10.1103/PhysRevB.100.115133

I. INTRODUCTION

Dirac and Weyl semimetals are a novel topological phase of matter that have attracted considerable interest [1–12]. The presence of topological phase confers these materials with novel properties such as anomalous and spin Hall conductivity [13–17], extremely large magnetoresistance and negative magnetoresistance [18–27], and ultrahigh carrier mobility [20,25,28]. The interband conductivity in the topological nontrivial material is expected to be universal: $\sigma_1(\omega) \propto \omega^{(d-2)/z}$, where d is the dimension of the system, z is the exponent in the band dispersion relation, $E(k) \propto |k|^z$ [2,7,29]. For example, two dimensions (e.g., graphene), with a linear dispersion of $E(k) \propto |k|$ (that is, $d = 2$ and $z = 1$), give rise to a frequency-independent conductivity, which has been confirmed by optical experiments [4]. For the case of a three-dimensional (3D) compound, such as pyrochlore iridates [5], Cd_3As_2 [6,7], $ZrTe_5$ [8,9], TaAs [10], and $YbMnBi_2$ [11,12], the linearly rising $\sigma_1(\omega)$ requires $\frac{d-2}{z} = 1$. By applying $d = 3$, a linear dispersion $z = 1$ is obtained, in good agreement with Dirac or Weyl semimetallic behavior.

Recently, rare-earth monoantimonides *R*Sb crystallized in a simple cubic rocksalt structure were shown to be compensated semimetals, with the conduction band mainly deriving from rare-earth $5d$ states and the valence band deriving from pnictogen $5p$ states, located at the Brillouin zone (BZ) center Γ and the BZ boundary X point, respectively [25,28,30–39]. Combining electronic structure with the exchange field induced by the f-electron degree of freedom, *R*Sb may therefore host topological phases of correlated electrons [40]. Dirac semimetal nodes or topological insulating gaps along Γ-X appearing in LaSb [31,36], the unusual fourfold-degenerate Dirac surface state in CeSb [32,37,38], and the Dirac-like structure at the Γ point in YSb, NdSb, and GdSb [32,35] make *R*Sb much more interesting. The properties of *R*Sb are further enriched by the reports of extremely large magnetoresistance in LaSb [25,28,30,31,39], PrSb [41], and LuSb [42] and in the antiferromagnetic semimetals NdSb [35] and CeSb [32,37,38].

Infrared spectroscopy is a powerful tool to study properties associated with topological materials. A previous optical spectroscopy study on *R*Sb focused on the high-frequency part of the spectroscopy, and a few reports are available for the low-frequency behavior and its temperature evolution. Our earlier work on LaSb revealed a well-formed plasma edge near 3000 cm^{-1} and a clear blueshift of the plasma edge with decreasing temperature [43]. However, no features are observed to be related to topological properties. In this paper, we present a systematic optical spectroscopy study of PrSb, an analog of LaSb, but with the presence of $4f$ electrons. We observe an increase of the plasma frequency ω_p with decreasing temperature, which is similar to LaSb [43]. In contrast to LaSb, two quasilinear segments with variable slopes are revealed in the real part of the optical conductivity $\sigma_1(\omega)$. In addition, theoretical calculations show band inversion at the X point. These findings may suggest nontrivial topological properties of PrSb.

II. EXPERIMENTAL DETAILS

High-quality single crystals of PrSb were grown by the self-flux method. The details of the sample synthesis can be found elsewhere [31]. Optical properties were measured on

*hong.xiao@hpstar.ac.cn

an as-grown shiny surface of the sample using a near-normal angle of incidence on Bruker 113v and Vertex 80v spectrometers. The spectral range spans from 50 to 20 000 cm^{-1}, and the data were collected at several selected temperatures between 10 and 300 K. The reflectivity $R(\omega)$ at each temperature was referenced to that of the gold/aluminum layer evaporated *in situ* on the sample surface. The real part of the optical conductivity $\sigma_1(\omega)$ was obtained with the Kramers-Kronig transformation of $R(\omega)$. Usually, for the low-frequency extrapolation, the Hagen-Rubens relation ($R = 1 - A\sqrt{\omega}$) is employed; for the high-frequency extrapolation, an extrapolation method with x-ray atomic scattering functions is used [44].

III. RESULTS AND DISCUSSION

Figure 1 shows the measured reflectivity $R(\omega)$ of PrSb at selected temperatures in the frequency range from 50 to 10 000 cm^{-1}. It is found that $R(\omega)$ steeply increases upon decreasing frequency and tends to 1 at low frequencies, which also increase with decreasing temperatures, indicating metallic behavior. In addition, a screened plasma edge appears at about 3000 cm^{-1}; the relatively low frequency of the screened plasma edge might be ascribed to its low carrier density. Note that two distinct peak features are observed in the reflectivity spectra at all temperatures: One is in the vicinity of the screened plasma edge; the other appears at higher-energy scales than the screened plasma edge, which is near 7000 cm^{-1}. Both of the peak features are rather broad and appear at a very high frequency, which cannot be related to phonon behavior; and the central frequencies have no temperature dependence, so these two peak features might be due to interband transitions.

With the appearance of interband transition in the vicinity of the screened plasma edge, it will broaden and shift the screened plasma edge in $R(\omega)$, making it very difficult for us to say precisely where the screened plasma edge occurs in $R(\omega)$. So we estimate the plasma frequency ω_p by calculating the low-frequency spectral weight (f-sum rule method), $\omega_p^2 = 8\int_0^{\omega_c}\sigma_1(\omega)d\omega$, where $\sigma_1(\omega)$ is the real part of the optical conductivity, shown in Fig. 2. The cutoff frequency ω_c is chosen to make the integration cover all contributions from free carriers and exclude contributions from interband transitions. Usually, the integral goes to a frequency where $\sigma_1(\omega)$ shows a minimum value; we expect there is a balance between the Drude component tail and the onset part of the interband transition. However, no distinct minimum value appears in $\sigma_1(\omega)$, so we choose $\omega_c = 1600$ cm^{-1}, as we can confirm that below this frequency, it is a Drude response and arises exclusively from free carriers. However, for frequency above 1600 cm^{-1}, the conductivity is relatively flat. Whether it arises from free carriers or interband transition is questionable. Therefore, we may underestimate the plasma frequency ω_p by this f-sum rule method. The plasma frequency ω_p obtained with this method is shown as the red line in Fig. 3(b).

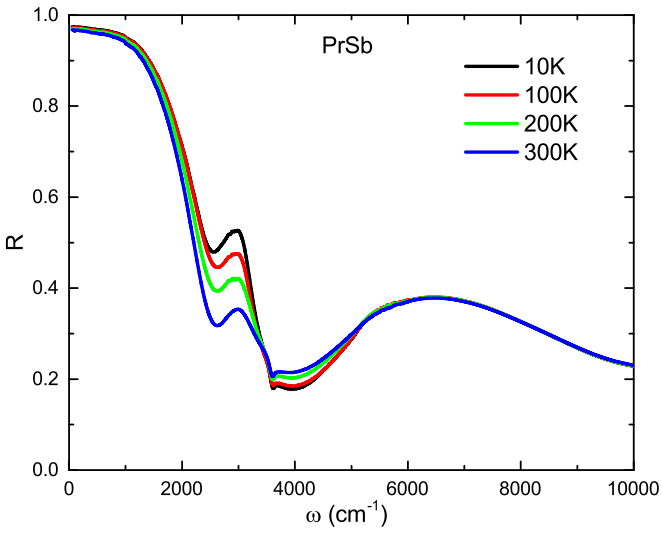

FIG. 1. The temperature-dependent $R(\omega)$ in the frequency range from 50 to 10 000 cm^{-1}.

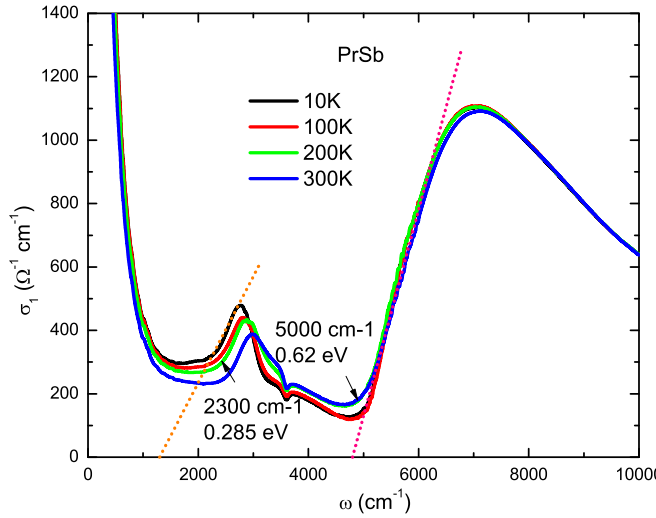

FIG. 2. The temperature-dependent optical conductivity $\sigma_1(\omega)$ of PrSb at several temperatures.

From Fig. 2, we can observe that the low-frequency $\sigma_1(\omega)$ (below about 1600 cm^{-1}) is dominated by the Drude-like response. In order to quantitatively analyze the low-frequency $\sigma_1(\omega)$, we fit it to the Drude model, which is used to describe the optical response of free carriers [45]:

$$\sigma_1(\omega) = \frac{2\pi}{Z_0}\frac{\omega_p^2}{\tau(\omega^2+\tau^{-2})}, \quad (1)$$

where Z_0 is the impedance of the free space, ω_p is the plasma frequency, and $1/\tau$ (that is, Γ) is the scattering rate of the carriers. We find that a single Drude component can fit the low-frequency $\sigma_1(\omega)$ well, as in Fig. 3(a), where we show the data for 300 K. The one-Drude-component model fit yields the temperature dependence of ω_p [shown as the blue line in Fig. 3(b)] and Γ [shown in Fig. 3(c)] for each temperature. We can observe that the obtained scattering rate Γ is about 180 cm^{-1} and increases with increasing temperature. However, the plasma frequency ω_p obtained with this method is about 1.5 times that obtained from the f-sum rule. The difference between their absolute values might be ascribed to two reasons: (1) the f-sum rule method may underestimate the

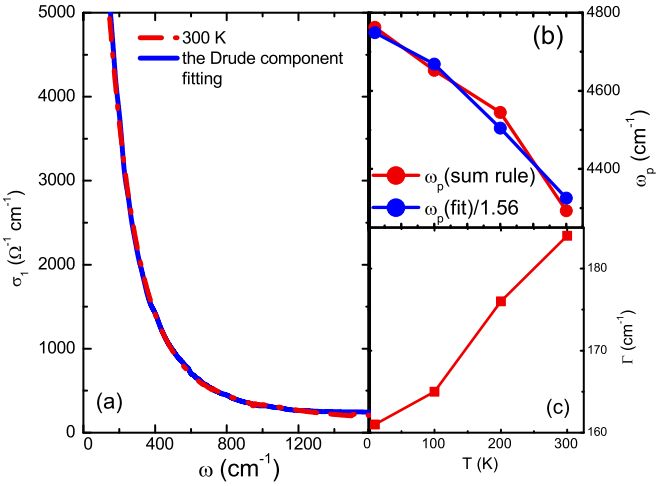

FIG. 3. (a) Fit (red dashed curve) to the optical conductivity (blue solid curve) in the frequency range of 0–1600 cm^{-1} at 300 K, which includes one Drude component. (b) The temperature dependence of the plasma frequency ω_P obtained from the fit and f-sum rule. (c) The temperature dependence of the scattering rate Γ obtained from the fit.

plasma frequency ω_p as explained above. (2) When we use a Drude component to fit the low-frequency optical conductivity, we may overestimate the contribution of the free carriers, as the fitted Drude tail above 1600 cm^{-1} would overestimate ω_p unavoidably. However, the plasma frequencies ω_p obtained with these two methods exhibit identical temperature dependence; that is, they increase as the temperature decreases.

We know that the plasma frequency satisfies the equation $\omega_P^2 = 4\pi ne^2/m^*$, where n is the carrier density and m^* is the effective mass. So the increase in ω_p indicates an increase of n/m^*. It is reported for HoSb that its carrier density decreases as the temperature decreases from 300 to 10 K [46]. Since PrSb is an isostructural compound of HoSb, the carrier density of the former could have a temperature dependence similar to that of the latter. Therefore, we attribute the increase of the plasma frequency to the decrease of the effective mass of carriers with decreasing temperature. The decrease of m^* in such low-carrier-density systems could be due to (i) the presence of a peculiar nonparabolic band and crossing E_F [47,48] and (ii) a heavy-electron band above but close to E_F [49], similar to the isostructural compound LaSb [43].

Above 1600 cm^{-1}, $\sigma_1(\omega)$ increases sharply, leading to a noticeable absorption edge, which is a signature of the emergence of interband transitions. Multiple absorption peaks arising from the interband transitions can be identified in the high-frequency $\sigma_1(\omega)$, shown as two broad peaks at about 2800 and 7000 cm^{-1}in $\sigma_1(\omega)$, respectively, corresponding to the two peak features in $R(\omega)$. Notably, two quasilinear components are observed in the frequency-dependent optical conductivity. One is between about 2300 and 2800 cm^{-1}(0.285–0.35 eV), depicted by the orange dotted line in Fig. 2; another ω-linear component with a different slope between about 5000 and 6200 cm^{-1} (0.62–0.78 eV) is denoted as the pink dotted line.

Linear optical conductivity is often associated with the linear dispersion in the electronic structures, as observed in 3D Dirac/Weyl semimetals [5–12]. Note that for the simplest case where the Dirac point is located right at the Fermi level, the interband conductivity results in a linear $\sigma_1(\omega)$, and it will pass through the origin. If the Fermi level is not at the Dirac point, the linear part of $\sigma_1(\omega)$ can still be extrapolated to the origin as $\omega \to 0$, but the interband transitions will be terminated below $\omega = 2\mu$ due to the blocking of the electronic states, where μ represents the chemical potential with respect to the Dirac point [10,50]. However, in some cases the data do not extrapolate to zero; instead, they extrapolate to a positive intercept on the vertical axis as $\omega \to 0$, possibly due to impurity scattering [51]. There are also cases in which the linear conductivity intercepts the photon-energy axis at $\omega \to 0$, as in the present study. The possible reasons are (i) a massless gap is opening in the Dirac/Weyl band structure [50–53] and (ii) the overlap of multiple interband transitions in Dirac/Weyl-like materials [54].

Our observation of two linear components is similar to the features in the topologically nontrivial material $YbMnBi_2$ [12], which was explained in the case of two nondegenerate Dirac cones shifted in reciprocal space by a finite reciprocal q vector [50]. The characteristic kink feature in $\sigma_1(\omega)$ was ascribed to the largest absorption between the two paired cones (which is a Van Hove singularity). It is the kink feature generated by the Van Hove singularity which breaks the expected linear frequency dependence of $\sigma_1(\omega)$ for a single Dirac cone into two quasilinear parts with variable slopes (associated with transitions connecting states with linear dispersion at the Dirac cones).

It is instructive to calculate the bulk band structure and simulate the optical conductivity of PrSb in order to get further evidence of the topological nontrivial property. Our calculations are performed using density functional theory (DFT) as implemented in the Vienna Ab initio Simulation Package (VASP) code [55,56]. The generalized-gradient approximation for the exchange correlation function is used. Throughout the work, the cutoff energy is set to be 400 eV for expanding the wave functions into plane-wave basis. In the calculation, the BZ is sampled in the k space within the Monkhorst-Pack scheme [57]. On the basis of the equilibrium structure, the k mesh used is $20 \times 20 \times 20$. In the calculations spin-orbital coupling is included, and the experimental parameters ($a = b = c = 4.5247$ Å in the primitive cell) [58] were used in calculation. The results are shown in Fig. 4. The band structure obtained from geometric relaxed optimized structural parameters is almost identical to the experimental parameter (see the Supplemental Material for details [59]). From Fig. 4(b), we find that these two peak features appear near 2080 and 7590 cm^{-1} (shown as two arrows). This is consistent with our experimental data, which have two peak features near 2800 and 7000 cm^{-1}. However, there is one additional peak feature near 4700 cm^{-1} in the theoretical calculation data. The difference between theoretical and experimental data might have two reasons: (1) our theoretical calculation is obtained at absolute zero temperature; (2) experimentally, the interband transition resulting in the two peak features near 2800 and 7000 cm^{-1} might be so strong that they obscure the contribution of the other interband transition. The features which appear in our experimental data also appear in our theoretical calculation data and make our explanation below much more reliable.

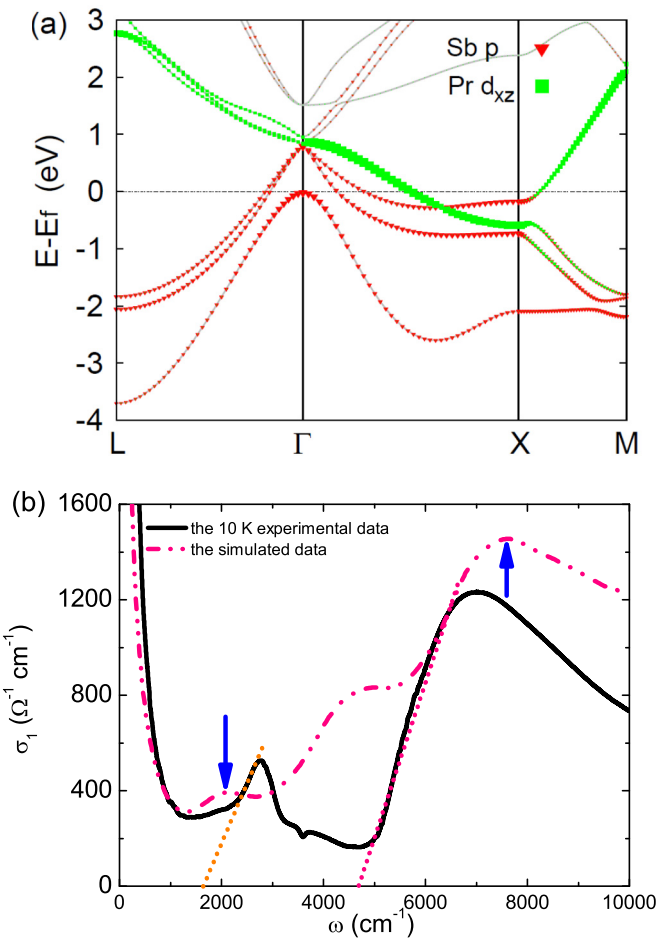

FIG. 4. (a) Band structure along high-symmetry directions of the Brillouin zone of PrSb. Red and green represent Sb 5*p* and Pr 5*d* orbitals, respectively. (b) The simulated optical conductivity of PrSb with a comparison of the experimental data for 10 K.

The calculated band structure is shown in Fig. 4(a). Here we focus on only the bands around the Fermi level. As can be seen, there are two holelike bands at the BZ center Γ point, and one electronlike band at the BZ boundary *X*. This is in accordance with the previous band-structure calculations for most *R*Sb compounds [28,30–33,35,37–40]. The small volume enclosed by the Fermi surface is in good agreement with the low carrier density revealed by our measured optical conductivity. Furthermore, the charge densities for the bands with energy −0.66 eV below the Fermi level at the *X* point mainly derive from the 5*d* states of Pr, while the bands with energy −0.16 eV below the Fermi level at the *X* point derive from the 5*p* states of Sb. The higher-energy (−0.16 eV) band with charges on the Sb atom and the lower-energy (−0.66 eV) band with charges on the Pr atom imply a band inversion at the *X* point, which is also revealed in LaSb [28,36] and LaBi [28]. The band inversion is a typical topologically nontrivial property manifested in the band structure, which is consistent with its topologically nontrivial property manifested in optical conductivity data.

Note that band 1 and band 2 in the Γ-*X* region near the Fermi level are nearly parallel. These kinds of "parallel bands" naturally give a peak in $\sigma_1(\omega)$ as states available to participate in interband transitions are huge, so this will result in the peak at about 2800 cm^{-1}. By the same argument, the peak at about 7000 cm^{-1} (0.87 eV) in $\sigma_1(\omega)$ results from the interband transition between the two parallel bands (band 1 and band 3). What's more, bands 1 and 2, which are associated with the band inversion, disperse almost linearly near the *X*-*M* region. It is natural to assign the observed second linear optical conductivity (shown as the pink dotted line of Fig. 2) to the interband transitions between these two bands. Further evidence can be revealed by a comparison of the onset energy of the linear optical conductivity and the band spacing between the two linear dispersion bands. The smallest band spacing between band 1 and band 2 near the *X*-*M* region has a value of 0.68 eV, which agrees well with the onset energies of the linear component within a reasonable error. It is also worth noting that the interband transitions from band 3 to band 1 near the *X*-*M* region may also make some contribution to the second linear optical conductivity, as band 3 also disperses linearly in this region. However, the frequency at which the conductivity deviates from linear dependence, which is 6200 cm^{-1} (0.78 eV), might be due to modification by other interband transitions, such as band 4 to band 1, etc. What's more, the first linear optical conductivity (shown as the orange dotted line in Fig. 2) might be ascribed to the interband transition superimposed on a Drude component tail.

IV. CONCLUSION

In conclusion, we have performed an optical spectroscopy study of PrSb single-crystal samples. It was found that the material has a low carrier density and the plasma frequency increases with decreasing temperature. More remarkably, we observed two quasilinear components with variable slopes in the real part of the optical conductivity $\sigma_1(\omega)$, which provides optical spectroscopic proof of the topological property of PrSb. In addition, the features in the optical conductivity can be interpreted well using a DFT band structure calculation.

ACKNOWLEDGMENT

The work is supported by NSAF, Grant No. U1530402, the National Basic Research Program of China (Grant No. 2017YFA0302901), the National Science Foundation of China (Grant No. 11674375).

[1] X. Wan, A. M. Turner, A. Vishwanath, and S. Y. Savrasov, Phys. Rev. B **83**, 205101 (2011).

[2] P. Hosur, S. A. Parameswaran, and A. Vishwanath, Phys. Rev. Lett. **108**, 046602 (2012).

[3] W. Witczak-Krempa and Y. B. Kim, Phys. Rev. B **85**, 045124 (2012).

[4] Z. Q. Li, E. A. Henriksen, Z. Jiang, Z. Hao, M. C. Martin, P. Kim, H. L. Stormer, and D. N. Basov, Nat. Phys. **4**, 532 (2008).

[5] A. B. Sushkov, J. B. Hofmann, G. S. Jenkins, J. Ishikawa, S. Nakatsuji, S. Das Sarma, and H. D. Drew, Phys. Rev. B **92**, 241108(R) (2015).

[6] A. Akrap, M. Hakl, S. Tchoumakov, I. Crassee, J. Kuba, M. O. Goerbig, C. C. Homes, O. Caha, J. Novák, F. Teppe, W. Desrat, S. Koohpayeh, L. Wu, N. P. Armitage, A. Nateprov, E. Arushanov, Q. D. Gibson, R. J. Cava, D. van der Marel, B. A. Piot, C. Faugeras, G. Martinez, M. Potemski, and M. Orlita, Phys. Rev. Lett. **117**, 136401 (2016).

[7] D. Neubauer, J. P. Carbotte, A. A. Nateprov, A. Löhle, M. Dressel, and A. V. Pronin, Phys. Rev. B **93**, 121202(R) (2016).

[8] Z.-G. Chen, R. Y. Chen, R. D. Zhong, J. Schneeloch, C. Zhang, Y. Huang, F. Qu, R. Yu, Q. Li, G. D. Gu, and N. L. Wang, Proc. Natl. Acad. Sci. USA **114**, 816 (2017).

[9] R. Y. Chen, S. J. Zhang, J. A. Schneeloch, C. Zhang, Q. Li, G. D. Gu, and N. L. Wang, Phys. Rev. B **92**, 075107 (2015).

[10] B. Xu, Y. M. Dai, L. X. Zhao, K. Wang, R. Yang, W. Zhang, J. Y. Liu, H. Xiao, G. F. Chen, A. J. Taylor, D. A. Yarotski, R. P. Prasankumar, and X. G. Qiu, Phys. Rev. B **93**, 121110(R) (2016).

[11] D. Chaudhuri, B. Cheng, A. Yaresko, Q. D. Gibson, R. J. Cava, and N. P. Armitage, Phys. Rev. B **96**, 075151 (2017).

[12] M. Chinotti, A. Pal, W. J. Ren, C. Petrovic, and L. Degiorgi, Phys. Rev. B **94**, 245101 (2016).

[13] J. Sinova, D. Culcer, Q. Niu, N. A. Sinitsyn, T. Jungwirth, and A. H. MacDonald, Phys. Rev. Lett. **92**, 126603 (2004).

[14] T. Rauch, H. Nguyen Minh, J. Henk, and I. Mertig, Phys. Rev. B **96**, 235103 (2017).

[15] R. Yu, W. Zhang, H.-J. Zhang, S.-C. Zhang, X. Dai, and Z. Fang, Science **329**, 61 (2010).

[16] S. Murakami, N. Nagaosa, and S.-C. Zhang, Science **301**, 1348 (2003).

[17] C.-Z. Chang, J. Zhang, X. Feng, J. Shen, Z. Zhang, M. Guo, K. Li, Y. Ou, P. Wei, L.-L. Wang, Z.-Q. Ji, Y. Feng, S. Ji, X. Chen, J. Jia, X. Dai, Z. Fang, S.-C. Zhang, K. He, Y. Wang, L. Lu, X.-C. Ma, and Q.-K. Xue, Science **340**, 167 (2013).

[18] A. A. Zyuzin, S. Wu, and A. A. Burkov, Phys. Rev. B **85**, 165110 (2012).

[19] I. Pletikosić, M. N. Ali, A. V. Fedorov, R. J. Cava, and T. Valla, Phys. Rev. Lett. **113**, 216601 (2014).

[20] X. Huang, L. Zhao, Y. Long, P. Wang, D. Chen, Z. Yang, H. Liang, M. Xue, H. Weng, Z. Fang, X. Dai, and G. Chen, Phys. Rev. X **5**, 031023 (2015).

[21] N. Kumar, C. Shekhar, S.-C. Wu, I. Leermakers, O. Young, U. Zeitler, B. Yan, and C. Felser, Phys. Rev. B **93**, 241106(R) (2016).

[22] J. Feng, Y. Pang, D. Wu, Z. Wang, H. Weng, J. Li, X. Dai, Z. Fang, Y. Shi, and L. Lu, Phys. Rev. B **92**, 081306(R) (2015).

[23] S. Sun, Q. Wang, P.-J. Guo, K. Liu, and H. Lei, New J. Phys. **18**, 082002 (2016).

[24] X. Wang, X. Pan, M. Gao, J. Yu, J. Jiang, J. Zhang, H. Zuo, M. Zhang, Z. Wei, W. Niu, Z. Xia, X. Wan, Y. Chen, F. Song, Y. Xu, B. Wang, G. Wang, and R. Zhang, Adv. Electron. Mater. **2**, 1600228 (2016).

[25] F. F. Tafti, Q. D. Gibson, S. K. Kushwaha, N. Haldolaarachchige, and R. J. Cava, Nat. Phys. **12**, 272 (2015).

[26] T. Liang, Q. Gibson, M. N. Ali, M. Liu, R. J. Cava, and N. P. Ong, Nat. Mater. **14**, 280 (2014).

[27] C. Shekhar, A. K. Nayak, Y. Sun, M. Schmidt, M. Nicklas, I. Leermakers, U. Zeitler, Y. Skourski, J. Wosnitza, Z. Liu, Y. Chen, W. Schnelle, H. Borrmann, Y. Grin, C. Felser, and B. Yan, Nature Phys. **11**, 645 (2015).

[28] P.-J. Guo, H.-C. Yang, B.-J. Zhang, K. Liu, and Z.-Y. Lu, Phys. Rev. B **93**, 235142 (2016).

[29] A. Bácsi and A. Virosztek, Phys. Rev. B **87**, 125425 (2013).

[30] L. K. Zeng, R. Lou, D. S. Wu, Q. N. Xu, P. J. Guo, L. Y. Kong, Y. G. Zhong, J. Z. Ma, B. B. Fu, P. Richard, P. Wang, G. T. Liu, L. Lu, Y. B. Huang, C. Fang, S. S. Sun, Q. Wang, L. Wang, Y. G. Shi, H. M. Weng, H. C. Lei, K. Liu, S. C. Wang, T. Qian, J. L. Luo, and H. Ding, Phys. Rev. Lett. **117**, 127204 (2016).

[31] X. H. Niu, D. F. Xu, Y. H. Bai, Q. Song, X. P. Shen, B. P. Xie, Z. Sun, Y. B. Huang, D. C. Peets, and D. L. Feng, Phys. Rev. B **94**, 165163 (2016).

[32] Y. Wu, Y. Lee, T. Kong, D. Mou, R. Jiang, L. Huang, S. L. Bud'ko, P. C. Canfield, and A. Kaminski, Phys. Rev. B **96**, 035134 (2017).

[33] L. Ye, T. Suzuki, C. R. Wicker, and J. G. Checkelsky, Phys. Rev. B **97**, 081108(R) (2018).

[34] A. Takayama, S. Souma, T. Sato, T. Arakane, and T. Takahashi, J. Phys. Soc. Jpn. **78**, 073702 (2009).

[35] N. Wakeham, E. D. Bauer, M. Neupane, and F. Ronning, Phys. Rev. B **93**, 205152 (2016).

[36] M. Zeng, C. Fang, G. Chang, Y.-A. Chen, T. Hsieh, A. Bansil, H. Lin, and L. Fu, arXiv:1504.03492.

[37] H. Oinuma, S. Souma, D. Takane, T. Nakamura, K. Nakayama, T. Mitsuhashi, K. Horiba, H. Kumigashira, M. Yoshida, A. Ochiai, T. Takahashi, and T. Sato, Phys. Rev. B **96**, 041120(R) (2017).

[38] N. Alidoust, A. Alexandradinata, S.-Y. Xu, I. Belopolski, S. K. Kushwaha, M. Zeng, M. Neupane, G. Bian, C. Liu, D. S. Sanchez, P. P. Shibayev, H. Zheng, L. Fu, A. Bansil, H. Lin, R. J. Cava, and M. Z. Hasan, arXiv:1604.08571.

[39] T. Kasuya, M. Sera, Y. Okayama, and Y. Haga, J. Phys. Soc. Jpn. **65**, 160 (1996).

[40] C. Guo, C. Cao, M. Smidman, F. Wu, Y. Zhang, F. Steglich, F.-C. Zhang, and H. Yuan, npj Quantum Mater. **2**, 39 (2017).

[41] F. Wu, C. Y. Guo, M. Smidman, J. L. Zhang, and H. Q. Yuan, Phys. Rev. B **96**, 125122 (2017).

[42] O. Pavlosiuk, M. Kleinert, P. Swatek, D. Kaczorowski and P. Wiśniewski, Sci. Rep. **7**, 12822 (2017).

[43] W.-J. Ban, W.-T. Guo, J.-L. Luo, and N.-L. Wang, Chin. Phys. Lett. **34**, 077804 (2017).

[44] D. B. Tanner, Phys. Rev. B **91**, 035123 (2015).

[45] Y. M. Dai, A. Akrap, J. Schneeloch, R. D. Zhong, T. S. Liu, G. D. Gu, Q. Li, and C. C. Homes, Phys. Rev. B **90**, 121114(R) (2014).

[46] Y.-Y. Wang, L.-L. Sun, S. Xu, Y. Su, and T.-L. Xia, Phys. Rev. B **98**, 045137 (2018).

[47] G. Li, W. Z. Hu, J. Dong, D. Qian, D. Hsieh, M. Z. Hasan, E. Morosan, R. J. Cava, and N. L. Wang, Phys. Rev. Lett. **99**, 167002 (2007).

[48] D. Tao, Y. Rui-Hua, S. You-Guo, and W. Nan-Lin, Chin. Phys. Lett. **30**, 127801 (2013).

[49] H. J. Park, L. J. Sandilands, J. S. You, H. S. Ji, C. H. Sohn, J. W. Han, S. J. Moon, K. W. Kim, J. H. Shim, J. S. Kim, and T. W. Noh, Phys. Rev. B **93**, 205122 (2016).

[50] C. J. Tabert and J. P. Carbotte, Phys. Rev. B **93**, 085442 (2016).
[51] C. J. Tabert, J. P. Carbotte, and E. J. Nicol, Phys. Rev. B **93**, 085426 (2016).
[52] B. Xu, L. X. Zhao, P. Marsik, E. Sheveleva, F. Lyzwa, Y. M. Dai, G. F. Chen, X. G. Qiu, and C. Bernhard, Phys. Rev. Lett. **121**, 187401 (2018).
[53] L. Benfatto and E. Cappelluti, Phys. Rev. B **78**, 115434 (2008).
[54] Y. Shao, Z. Sun, Y. Wang, C. Xu, R. Sankar, A. J. Breindel, C. Cao, M. M. Fogler, A. J. Millis, F. Chou, Z. Li, T. Timusk, M. B. Maple, and D. N. Basov, Proc. Natl. Acad. Sci. USA **116**, 1168 (2019).
[55] G. Kresse and J. Hafner, Phys. Rev. B **47**, 558 (1993).
[56] G. Kresse and J. Furthmüller, Phys. Rev. B **54**, 11169 (1996).
[57] H. J. Monkhorst and J. D. Pack, Phys. Rev. B **13**, 5188 (1976).
[58] O. V. Zhak and N. V. Malyus, Inorg. Mater. **42**, 976 (2006).
[59] See Supplemental Material at http://link.aps.org/supplemental/10.1103/PhysRevB.100.115133 for details of the band structure. .